PAPER • **OPEN ACCESS**

Gradual reset and set characteristics in yttrium oxide based resistive random access memory

To cite this article: Stefan Petzold *et al* 2019 *Semicond. Sci. Technol.* **34** 075008

OPEN ACCESS
IOP Publishing
Semiconductor Science and Technology
Semicond. Sci. Technol. **34** (2019) 075008 (6pp)
https://doi.org/10.1088/1361-6641/ab220f

Gradual reset and set characteristics in yttrium oxide based resistive random access memory

Stefan Petzold[1], Eszter Piros[1], S U Sharath[1], Alexander Zintler[2], Erwin Hildebrandt[1], Leopoldo Molina-Luna[2], Christian Wenger[3] and Lambert Alff[1]

[1] Advanced Thin Film Technology Division, Institute of Materials Science, Technische Universität Darmstadt, 64287 Darmstadt, Germany
[2] Advanced Electron Microscopy Division, Institute of Materials Science, Technische Universität Darmstadt, 64287 Darmstadt, Germany
[3] IHP—Leibniz-Institut fuer innovative Mikroelektronik, 15236 Frankfurt (Oder), and Brandenburg Medical School Theodor Fontane, 16816 Neuruppin, Germany

E-mail: petzold@oxide.tu-darmstadt.de

Received 28 January 2019, revised 8 April 2019
Accepted for publication 16 May 2019
Published 12 June 2019

Abstract

This paper addresses the resistive switching behavior in yttrium oxide based resistive random access memory (RRAM) (TiN/yttrium oxide/Pt) devices. We report the coexistence of bipolar and unipolar resistive switching within a single device stack. For bipolar DC operation, the devices show gradual set and reset behavior with resistance ratio up to two orders of magnitude. By using nanosecond regime pulses (20 to 100 ns pulse width) of constant voltage amplitude, this gradual switching behavior could be utilized in tuning the resistance during set and reset spanning up to two orders of magnitude. This demonstrates that yttrium oxide based RRAM devices are alternative candidates for multibit operations and neuromorphic applications.

Keywords: gradual, neuromorphic, resistive random access memory, resistive switching, retention, yttria, yttrium oxide

(Some figures may appear in colour only in the online journal)

1. Introduction

Resistive random access memory (RRAM) has attracted a lot of attention for more than a decade, as a promising candidate for the next generation of non-volatile memories. Traditional flash memory has reached the lateral scaling limit [1] and current approaches for further scaling are limited to the third dimension [2]. The steadily growing market of information communication technology [3] keeps a continuous pressure on developing power efficient, high-density memories at low cost. There are several suited materials exhibiting resistive switching [4], such as TiO_2, HfO_2, TaO_x, Ga_2O_3 [5] or mixed systems like $Ba_{0.6}Sr_{0.4}TiO_3$ [6] or In-Ga-Zn-O [7]. Although belonging to the group of rare earths, yttrium is not considered to belong to the group of critical materials by representing about 31 ppm of the Earth crust [8]. Due to its dielectric constant of 14–17 [9–11], wide band gap of 5.5 to 6.2 eV [12–14], high breakdown voltage and high conduction band off-set [15], yttrium oxide was considered as a possible candidate to replace SiO_2 as gate dielectric for field effect transistors [16, 17] amongst other high-k candidates, such as HfO_2, ZrO_2, Al_2O_3, Ta_2O_5. Therefore, yttria was intensively investigated in terms of growth on Si/SiO_2 establishing different atomic layer deposition (ALD) processes [18–20] and creating the basis for complementary metal-oxide-

semiconductor-compatibility. Similar to hafnia, Y_2O_3 is described in the literature as a fast ion conductor [15]. Experiments on bulk Y_2O_3 have revealed activation energies for oxygen diffusion as low as 19.580 cal/mol (0.85 eV) [21] being related to the defective structure of the body centered sesquioxide where one fourth of the anion sublattice sites remain unoccupied. The valence state of +3 is considered to be the only stable oxidation state for yttrium. Its initially defective structure makes Y_2O_3 interesting for investigating its resistive switching behavior. Lately, RRAM becomes a more and more attractive candidate for neuromorphic applications due to its ability to show learning and forgetting processes [22, 23] by mimicking analog synaptic weights. In principle, a synapse resembles a two-terminal device in which the resistance can be incrementally modulated [24]. Therefore, a possible way to mimic the functionality of the human brain is by using a network of massively parallelized memristors with high connectivity. This approach enables overcoming drawbacks of the von Neumann architecture in terms of data centric applications such as real time language or data recognition [25]. Yao *et al* [26] demonstrated face classification utilizing a 1024-cell-1T1R RRAM based neuromorphic network with analogously tunable resistance being x1000 (x20) more energy efficient than using an Intel Xeon Phi processor with off-chip storage (with on-chip integrated digital RRAM). Forecasts suggest a future computational efficiency of integrated on chip memristors of over 100 trillion operations per second per Watt [27]. Even memristors on flexible substrates which are interesting for applications in wearable electronic devices or foldable displays have recently been reported to show synaptic characteristics [28]. For neuromorphic applications, the ideal candidate needs to provide gradual set and reset operations with accessibility to a high density of resistance states. In other terms, a linear analogously/continuously variable conductance in a high on/off ratio range with multi-level feasibility is desired. Additionally, due to the desired high device density, a low power consumption [29] (e.g. by low operation voltages with short pulses) while maintaining the stability of the resistance states (high temperature data retention, endurance, and immunity to noise) [30] is important, demanding further material optimization by engineering.

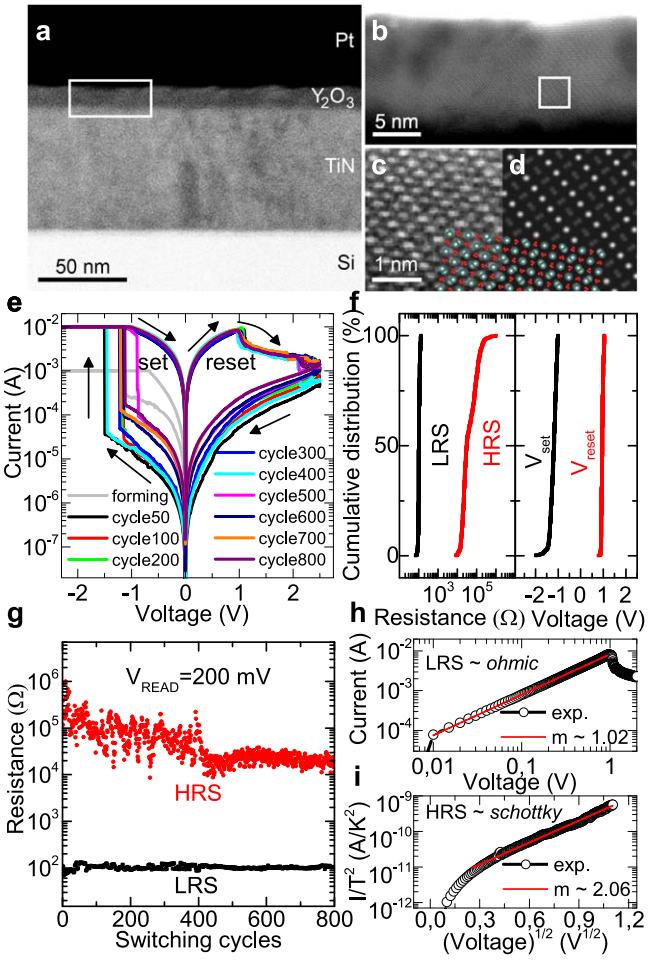

Figure 1. (a) BF-STEM image showing the thin film stack; (b) HAADF-STEM showing a polycrystalline Y_2O_3 layer, grain size coincides with layer thickness; (c) High resolution HAADF-STEM image of a single Y_2O_3 grain (source marked in (b)), Wien filtered; (d) QSTEM simulation along (010), (101) facing up (growth direction); (e) Bipolar resistive switching behavior of yttria taken after a forming step; (f) Cumulative probability distributions of (left) resistance in HRS and LRS and (right) set and reset voltages; (g) Endurance plot of the bipolar resistive switching for more than 800 cycles with an average and minimum ratio of 640 and 80, respectively; (h) Ohmic and (i) Schottky-type conduction behavior of LRS and HRS, respectively.

2. Experimental

The devices under test (DUT) consist of TiN/Y_2O_3/Pt (see figure 1(a)). The TiN layers with thickness of 70 nm were reactively deposited on (100) Si-wafers using direct current (DC) magnetron sputtering of Ti and nitrogen as reactive gas at room temperature. The 12 nm thick polycrystalline Y_2O_3-layer has been grown by elemental e-beam evaporation of yttrium at 450 °C. *In situ* oxidation has been achieved using RF-activated oxygen radicals from a radical source allowing for oxygen engineering of the dielectric layer [31]. The top electrode (TE) was deposited by sputtering 100 nm of platinum using a DC sputter coater. After sputtering the TE, the samples were subjected to a standard lithography step using a lift-off process in order to produce metal-insulator-metal (MIM) devices of 30 × 30 μm^2 size. Electrical characterization was done using a Keithley 4200 semiconductor characterization system (SCS) by biasing the TE (here Pt) and using the internal current compliance (CC) of the SCS to prevent device hard breakdown. All pulse operations were performed consistently with 20 ns for fall and rise time, respectively. Retention measurements were performed using an oven at 85 °C in ambient atmosphere. Scanning transmission electron microscopy was performed using a JEOL JEM ARM-200F.

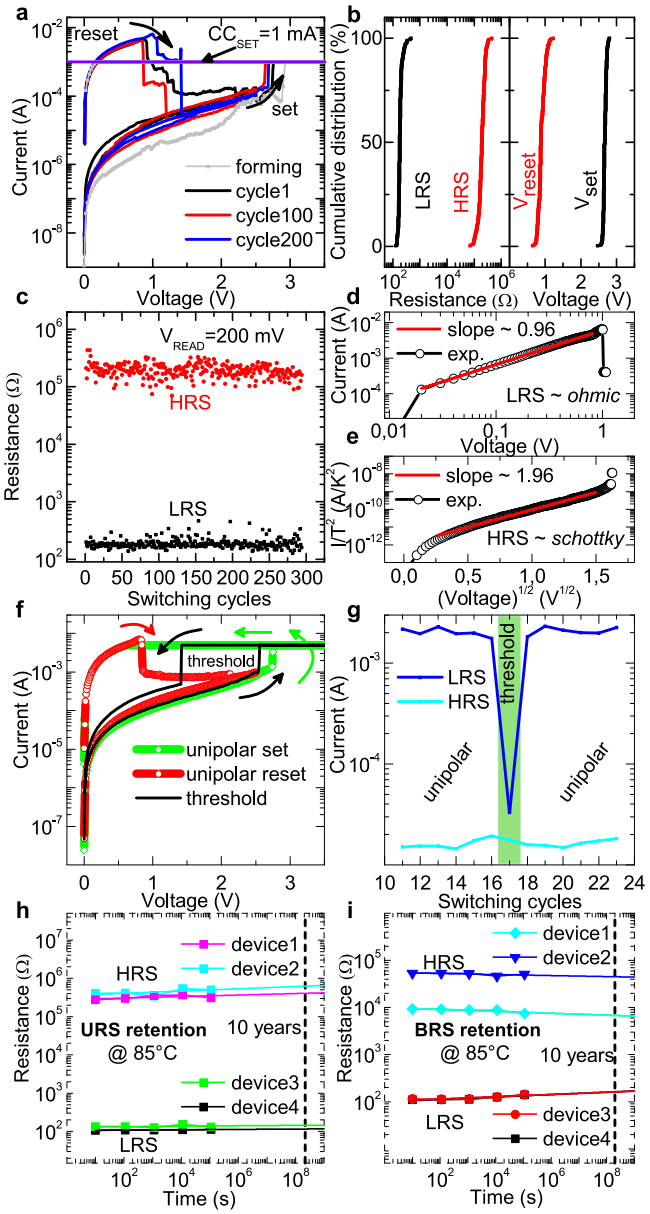

Figure 2. (a) Unipolar resistive switching behavior over 200 DC cycles of Y_2O_3 (In gray: initial electroforming step); (b) Cumulative probability distributions in the unipolar device for (left) resistance states in HRS and LRS and (right) set and reset voltages; (c) Endurance plot of the unipolar device taken at $V_{READ} = 200$ mV; *I*–*V*-curves for the unipolar device in (d) low and (e) high resistive states dominated by ohmic (m 0.96) and Schottky (m 1.96) behavior, respectively; (f) Coexistence of unipolar and threshold switching in the same device; (g) Unipolar switching recovers after intermittent threshold switching. Retention characteristics of (h) the unipolar and (i) the bipolar resistive switching devices. Different devices were put in either high or low resistive state and then exposed to 85 °C for different periods of time.

3. Results and discussion

Shown in figure 1(a) is a bright-field scanning transmission electron microscopy (BF-STEM) image of the complete film layer stack. Figure 1(b) reveals a polycrystalline structure in the yttria film (inset of figure 1(a)). The highlighted area of figure 1(b) is shown in figures 1(c) and (d): High-resolution high-angle annular dark-field (HAADF-STEM) image and corresponding QSTEM simulation [32] of a cubic (101) oriented grain. A Vesta [33] rendering was inserted for visualization (color coding: yttrium—cyan, oxygen—red). X-ray diffraction measurements show a coexistence of monoclinic (40$\bar{2}$) and cubic (222) and (400) phases, respectively. In this section, we also present the *I*–*V* characterization results acquired in DC sweeping mode. The switching cycles shown in figure 1 were obtained by applying voltage to the Pt top electrode while keeping the TiN bottom electrode grounded. In the scarce literature about yttria-based RRAM, so far only either unipolar [34] or bipolar [35] switching has been reported. Here, we report for the first time the observation of both bipolar (BRS) and unipolar resistive switching (URS) modes in the same stack configuration based on yttrium oxide which can be deliberately accessed by choosing the voltage polarity. The observed switching is attributed to the valence change mechanism (VCM). The conductive filament (CF) is believed to consist of a high local density of oxygen vacancies promoting current transport through the dielectric layer. If the CF is connected to both electrodes the device is considered to be in a low resistive state (LRS). By rupturing the CF, the device can be put into a high resistive state (HRS). Considering the voltage polarity of the electroforming and set process in the BRS operation, oxygen within the dielectric layer is driven towards the TiN electrode oxidizing the anode [36], thus, creating oxygen vacancies in the yttria layer. During filament formation, TiO_xN_{1-x} will form at the TiN/Y_2O_{3-x}-interface [37], later acting as an oxygen reservoir for the following reset procedure. While the process in the BRS is believed to be mainly field driven, the switching process in the URS mode is more dependent on Joule heating effects and diffusion along concentration and temperature gradients and resulting Soret forces [38]. URS can mostly be found for stack combinations with inert electrode materials such as platinum [39]. Occasional threshold resistive switching (TRS) could also be identified and was found to coexist within the URS cycles similar as reported previously for hafnium oxide [38].

For the bipolar operation, the electroforming occurred in negative voltage polarity (−1.19 V) with an applied current compliance of 1 mA (see figure 1(e)). All tested devices were found to be forming-free showing an average forming voltage of −1.58 V with a standard deviation of 0.55 V (for the overall 42 investigated devices for BRS) suggesting a sub-stoichiometric Y_2O_{3-x} composition [40, 41]. Forming-free devices in yttria have been previously reported in literature [35] and have been correlated to a facilitated filament formation along the [110] direction of the cubic phase [42]. Considering the cubic orientation of the film, the grain size being in the same order as the dielectric layer, and the growth direction (see figures 1(b)–(d)), the observed forming-free behavior is consistent with the reported vacancy chains along [110]. During the set process, occasional intermediate steps were observed in the otherwise abrupt switching. Reset in BRS was found to be mostly gradual making yttrium oxide based devices interesting for synaptic applications.

From an application point of view, it is important to address the variability and reliability of the switching devices. Figures 1(f) (and 2(b)) show the empirical cumulative distribution function F(x) calculated as the number of observations less than or equal to x divided by the total number of observations n. Figure 1(f) (left) shows the R_{HRS} and R_{LRS} distributions taken at −200 mV readout voltage. From the cumulative distributions of the operation voltages (figure 1(f) (right)), it is clear that set occurs mostly at ≈ −1 V and that the reset voltages show little deviation from the mean value of 0.97 V. The LRS is uniform, the off state, however, shows enhanced variability. This is most likely due to the fact that we use a limited voltage range to reduce the device hard breakdown (by setting the device in URS mode without applied CC) possibility, thus, hindering a deeper reset. This is also depicted in the endurance data (figure 1(g)) from which it can be seen that during the first 400 DC cycles resistance values in HRS show enhanced variability. During these cycles, R_{HRS} gradually settles and fluctuations are reduced. Overall, the cycle-to-cycle variation is low for both the operation voltages and the resistance values measured in HRS and LRS during the plotted 800+ DC cycles. The resistance ratio's average value of ≈640 and minimum of 80 ensure error-free data readout. By operating in pulse mode and restraining the pulse width to 100 ns, higher reset voltages could be applied without activating a unipolar set, thus enabling deeper resets as can be seen in figure 3(d). The conduction mechanism was found to show ohmic behaviour in the LRS (figure 1(h)) and be consistent with the Schottky-mechanism in HRS (figure 1(i)).

The same characterization was carried out for the unipolar switching mode (see figure 2(a)). The URS has been achieved by applying positive voltage on the Pt electrode. The DUT shows uniform on-off resistance (left) and operation voltage distributions (right) (figure 2(b)). Set happens at ≈2.7 V and reset at ≈1 V. The operation voltage distributions show overall small variations. Resistance taken at 200 mV readout voltage in the LRS is in the range of 10^2 Ω, while the HRS resistance falls in the range of 10^5 Ω. The cumulative probability plot shows narrow resistance distributions in both LRS and HRS. Figure 2(c) shows the endurance data taken for 250+ DC switching cycles. The resistance in both resistive states shows uniform performance with extremely low cycle-to-cycle variability. The average on-off-ratio was found to be ≈1060 and during switching a minimal ratio of 240 was maintained. The conduction behavior of the unipolar device was found to be ohmic in the LRS and to be dominated by Schottky-emission in the HRS, as shown in figures 2(d) and (e), respectively. TRS was found to occasionally occur in the unipolar cycles. In figure 2(f) the *I*–*V* curves of such a device are depicted. During threshold switching, the current abruptly switches in response to increasing voltages, upon decreasing bias, however, this higher current level becomes unstable below a critical voltage and the device crosses over into the HRS again. As can be seen from the endurance plot depicted in figure 2(g), unipolar switching shows an instability towards the aforementioned TRS which, however, cannot be stabilized. This instability has been attributed to insufficient heat

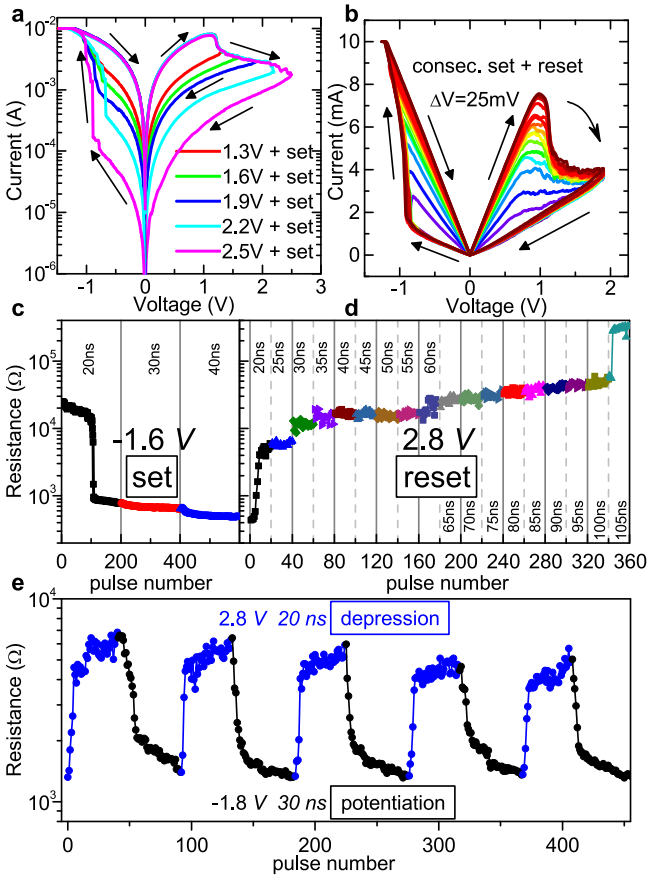

Figure 3. (a) Successive positive voltage sweeps with increasing maximum value ('write') and corresponding negative voltage sweeps ('erase') in the bipolar device. The transition from LRS to HRS is reproducibly controllable through intermediate resistance states. The current levels are well distinguishable. (b) Tuning of LRS levels can be achieved by using consecutive set and reset steps. (c) Pulse setting with varying pulse width ranging from 20 to 40 ns. (d) Pulse resetting with stepwise increasing pulse width by 5 ns from 20 to 105 ns. (e) five consecutive pulse depression/potentiation cycles with constant pulse width, voltage amplitude, and pulse number (50 pulses of depression and 40 pulses for potentiation) showing ratios up to 5.

dissipation [43] and, therefore, can be described as a write error. In 400 nm thick polycrystalline titanium oxide films, the spontaneous dissolution of the CF upon reducing the electric field was related to thermal diffusion assisted by the repelling coulombic forces of the ionized vacancies [44].

As mentioned before, the dominant conduction mechanism was investigated under both bipolar and unipolar operation. The low resistive state shows ohmic behavior for both BRS and URS as shown in figures 1(h) and 2(d), respectively, with a slope of ≈1 in double-logarithmic depiction of the *I*–*V* curves. The HRS, however, was found to be dominated by the Schottky-mechanism in bipolar, as well as in unipolar switching mode. The Schottky-type conduction is described by [45]

$$I = AT^2 \exp\{(\beta V^{1/2} - \Phi)(\mathrm{kT})^{-1}\} \quad (1)$$

$$\beta = (e^3/4\pi\varepsilon_0\varepsilon_r)^{1/2} \quad (2)$$

where A is the Richardson constant, T is the absolute

temperature, Φ is the barrier height, k is Boltzmann's constant, e is the elementary charge, ε_0 is the permittivity of free space and ε_r is the relative permittivity. Typically, a Schottky-contact forms at electrodes with high work function, resulting in a rectifying behavior. For BRS, we have observed such diode-like behavior with a high non-linearity of ≈10 for opposite bias polarities, which is especially pronounced in the first 400 DC cycles (figure 1(e)). Here, the current is about one order of magnitude higher under positive bias than for the negative voltage direction, suggesting the formation of a dominant Schottky-barrier at the Pt electrode [46]. Similar tendencies were found for yttria-based RRAM devices with another high work function electrode, namely Ruthenium [35] and for $TiN/SrTiO_3/Pt$ devices [47]. Additionally, the $\ln(I/T^2) - V^{1/2}$ plot shows the expected linear behavior (figures 1(i) and 2(e)) allowing for the extraction of the barrier height which was found to be ≈1.00 eV at the correlated Y_2O_3/Pt junction. In the case of URS, the calculated barrier height of ≈1.06 eV is very similar to the value obtained in BRS. The observed conduction mechanism and barrier heights are in good agreement with results obtained on $Metal/Y_2O_3/Pt$ devices [48].

Figures 2(h) and (i) show the results of high temperature data retention measurements obtained at 85 °C for four URS and BRS devices, respectively. The ten year extrapolation shows that data is retained in the measured cells in both HRS and LRS in both switching modes. In the case of the devices which were operated in the unipolar mode, resistance is barely changed and shows almost no degradation in all measured devices. The devices operated in a bipolar mode also exhibit promising retention characteristics. The two different resistance states of the HRS seen in figure 2(i) represent devices with different stresses, where 'device1' was cycled approximately 200 cycles more than 'device 2'.

One possible way to achieve higher data density is the realization of multi-bit storage in RRAM. This is usually carried out by stabilizing multiple current levels by either varying current compliance during the set or controlling the reset voltages. The gradual reset seen in the bipolar device allows for reproducible control of the transition from LRS to HRS through stable intermediate high resistance states. One method to achieve these states is shown in figure 3(a). First, the DUT was brought into LRS with a negative voltage sweep to −2.5 V. Then, starting from this LRS, the voltage was swept from +1.3 V to +2.5 V in 0.3 V increments ('write' operation, reset process in BRS mode) with a consecutive voltage sweep to −2.5 V after each positive sweep to enter the LRS state again ('erase' operation, set process in BRS mode). During this operation sequence, the intermediate resistance states were found to be stable and well reproducible. When plotting the data in linear scale (figure 3(b)) in the range up to 1.9 V for the reset voltage the gradual character becomes obvious not only in the reset process, but also in the set process. As shown in figure 3(b), this behavior can be used to access intermediate states also by consecutively varying the set voltage. Thereby, the devices can be operated by systematically increasing set steps followed by consecutive individual resets. Overall, this allows for accessing different resistance states by set and reset processes, enabling multilevel operations. This gradual switching behavior can also be accessed by using pulse stimuli as employed for practical memory as well as neuromorphic applications as shown in figures 3(c)–(e), respectively. Here, the resistance could be modulated by applying pulse stimuli with constant voltage amplitudes (2.8 V for reset and −1.6 V for set). Resistance ratios of over more than two orders of magnitude for reset and almost two orders of magnitude for set could be achieved. In the experiment, only the pulse width is varied from as low as 20 ns up to 105 ns pulses as displayed in figures 3(c) and (d), respectively. For synaptic applications, the synaptic weight, here resistance, could also be changed reproducibly as a function of fixed numbers of pulse stimuli with constant pulse width for potentiation (40 pulses with −1.8 V for 30 ns) and depression (50 pulses with 2.8 V for 20 ns). In this example (figure 3(e)), the device is shown to run through 5 consecutive cycles of weight increase followed by weight decrease with an overall resistance ratio of about 5.

4. Conclusion

In this study, we report for the first time the coexistence of bipolar resistive switching and unipolar resistive switching within one stack combination based on yttrium oxide. The URS is characterized by a high on-off-ratio with low switching variability, excellent data retention and DC endurance. In both BRS and URS, the conduction behavior of LRS and HRS have been identified as ohmic conduction and Schottky emission, respectively. The BRS is characterized by low variability, good data retention, high DC endurance, and average on-off-ratio above 100. Additionally, the obtained concurrent gradual transitions during BRS set and reset which have been employed in pulse depression and potentiation operations with shown plasticity over about two orders of magnitude make RRAM based on yttrium oxide an interesting alternative candidate for neuromorphic synapses. Combined with its characteristic of being forming-free and having low operation voltages, RRAM based on yttrium oxide is highlighted as a suitable material candidate for new high density non-volatile memory technologies. The reported forming-free behavior has been related to a preferential defect chain along the [110] direction of the cubic yttria phase and should be further investigated in future.

Acknowledgments

This work was supported by the Deutscher Akademischer Austauschdienst (DAAD) and the Deutsche Forschungsgemeinschaft under project AL 560/13-2. Funding by the Federal Ministry of Education and Research (BMBF) under contract 16ES0250 and 16ESE0298, and by ENIAC JU within the project PANACHE is gratefully acknowledged. The work leading to this publication has been undertaken in the framework of the WAKeMeUP project which received funding from the Electronic Components and Systems for

European Leadership Joint Undertaking in collaboration with the European Union's H2020 Framework Programme (H2020/2014-2020) and National Authorities, under grant agreement n° 783176. Also, funding from DFG grant MO 3010/3-1 and the European Research Council (ERC) 'Horizon 2020' Program under Grant No. 805359-FOXON are gratefully acknowledged.

ORCID iDs

Stefan Petzold https://orcid.org/0000-0002-4994-9781

References

[1] Iwai H 2008 Cmos technology after reaching the scale limit *Junction Technology, 2008. IWJT'08. Extended Abstracts-2008 8th International workshop on (IEEE)* 1–2
[2] Wong H S P, Lee H Y, Yu S, Chen Y S, Wu Y, Chen P S, Lee B, Chen F T and Tsai M J 2012 *Proc. IEEE* 100 1951–70
[3] Bez R 2005 *Microelectron. Eng.* **80** 249–55 14th biennial Conference on INFOS2005
[4] Pan F, Gao S, Chen C, Song C and Zeng F 2014 *Mater. Sci. Eng. R Rep.* **83** 1–59
[5] Yan X, Hao H, Chen Y, Li Y and Banerjee W 2014 *Appl. Phys. Lett.* **105** 093502
[6] Yan X, Li Y, Zhao J, Li Y, Bai G and Zhu S 2016 *Appl. Phys. Lett.* **108** 033108
[7] Yan X, Hao H, Chen Y, Shi S, Zhang E, Lou J and Liu B 2014 *Nanoscale Res. Lett.* **9** 548
[8] Cotton S A 2006 *Encyclopedia of Inorganic Chemistry* (https://doi.org/10.1002/0470862106.ia211)WorldCat: https://www.worldcat.org/title/scandium-yttrium-the-lanthanides-inorganic-coordination-chemistry/oclc/7321828802
[9] Gurvitch M, Manchanda L and Gibson J 1987 *Appl. Phys. Lett.* **51** 919–21
[10] Pal S, Ray S, Chakraborty B, Lahiri S and Bose D 2001 *J. Appl. Phys.* **90** 4103–7
[11] Gusev E, Cartier E, Buchanan D, Gribelyuk M, Copel M, Okorn-Schmidt H and D'Emic C 2001 *Microelectron. Eng.* **59** 341–9
[12] de Rouffignac P, Park J S and Gordon R G 2005 *Chem. Mater.* **17** 4808–14
[13] Marsella L and Fiorentini V 2004 *Phys. Rev.* B **69** 172103
[14] Wallace R M and Wilk G 2002 *MRS Bull.* **27** 186–91
[15] Robertson J 2000 *J. Vac. Sci. Technol.* B **18** 1785–91
[16] Sharma R K, Kumar A and Anthony J M 2001 *JOM* **53** 53–5
[17] He G, Zhu L, Sun Z, Wan Q and Zhang L 2011 *Prog. Mater. Sci.* **56** 475–572
[18] Niinistö J, Putkonen M and Niinistö L 2004 *Chem. Mater.* **16** 2953–8
[19] Putkonen M, Sajavaara T, Johansson L S and Niinistö L 2001 *Chem. Vap. Deposition* **7** 44–50
[20] Park I S, Jung Y C, Seong S, Ahn J, Kang J, Noh W and Lansalot-Matras C 2014 *J. Mater. Chem.* C **2** 9240–7
[21] Berard M, Wirkus C and Wilder D 1968 *J. Am. Ceram. Soc.* **51** 643–7
[22] Yan X, Zhou Z, Ding B, Zhao J and Zhang Y 2017 *J. Mater. Chem.* C **5** 2259–67
[23] Yan X, Zhang L, Chen H, Li X, Wang J, Liu Q, Lu C, Chen J, Wu H and Zhou P 2018 *Adv. Funct. Mater.* **28** 1803728
[24] Jo S H, Chang T, Ebong I, Bhadviya B B, Mazumder P and Lu W 2010 *Nano Lett.* **10** 1297–301
[25] Burr G W *et al* 2017 *Advances in Physics:* X **2** 89–124
[26] Yao P *et al* 2017 *Nat. Commun.* **8** 15199
[27] Hu M *et al* 2018 *Adv. Mater.* **30** 1705914
[28] Yan X, Zhou Z, Zhao J, Liu Q, Wang H, Yuan G and Chen J 2018 *Nano Res.* **11** 1183–92
[29] Rajendran B, Liu Y, Seo J S, Gopalakrishnan K, Chang L, Friedman D J and Ritter M B 2013 *IEEE Trans. Electron Devices* **60** 246–53
[30] Ielmini D 2018 *Microelectron Eng.* **190** 44–53
[31] Sharath S U, Kurian J, Komissinskiy P, Hildebrandt E, Bertaud T, Walczyk C, Calka P, Schroeder T and Alff L 2014 *Appl. Phys. Lett.* **105** 073505
[32] Koch C T 2002 Determination of core structure periodicity and point defect density along dislocations *PhD Thesis* Arizona State University https://ui.adsabs.harvard.edu/abs/2002PhDT.....50K/ https://www.worldcat.org/title/determination-of-core-structure-periodicity-and-point-defect-density-along-dislocations/oclc/52148964
[33] Momma K and Izumi F 2011 *J. Appl. Crystallogr.* **44** 1272–6
[34] Pi C, Ren Y, Liu Z Q and Chim W K 2012 *Electrochem. Solid State Lett.* **15** G5–7
[35] Pan T M, Chen K M and Lu C H 2011 *Electrochem. Solid State Lett.* **14** H27–9
[36] Valov I 2017 *Semicond. Sci. Technol.* **32** 093006
[37] Guan X *et al* 2012 *IEEE Trans. Electron Devices* **59** 1172–82
[38] Sharath S U *et al* 2017 *Adv. Funct. Mater.* **27**
[39] Kamiya K, Yang M Y, Nagata T, Park S G, Magyari-Köpe B, Chikyow T, Yamada K, Niwa M, Nishi Y and Shiraishi K 2013 *Phys. Rev.* B **87** 155201
[40] Sharath S U, Joseph M, Vogel S, Hildebrandt E, Komissinskiy P, Kurian J, Schröder T and Alff L 2016 *Appl. Phys. Lett.* **109** 173503
[41] Sharath S U *et al* 2014 *Appl. Phys. Lett.* **104** 063502
[42] Rushchanskii K Z, Blügel S and Ležaić M 2019 Faraday discussions **213** 321
[43] Yang J J, Strukov D B and Stewart D R 2013 *Nat. Nanotechnol.* **8** 13
[44] Hossein-Babaei F and Alaei-Sheini N 2016 *Sci. Rep.* **6** 29624
[45] Basak D and Sen S 1995 *Thin Solid Films* **254** 181–6
[46] Yan X, Xia Y, Xu H, Gao X, Li H, Li R, Yin J and Liu Z 2010 *Appl. Phys. Lett.* **97** 112101
[47] Fleck K, La Torre C, Aslam N, Hoffmann-Eifert S, Böttger U and Menzel S 2016 *Phys. Rev. Applied* **6** 064015
[48] Mikhaelashvili V, Betzer Y, Prudnikov I, Orenstein M, Ritter D and Eisenstein G 1998 *J. Appl. Phys.* **84** 6747–52